Determination of the Optimum Joint Design for LENS Fabricated Ti6Al4V and Ti6Al4V/TiC Dual-Material Structures

Obielodan J.O[1] and Stucker B.E[2]*

[1]Mechanical and Aerospace Engineering Department, Utah State University, Logan, UT 84322

[2]Industrial Engineering Department, University of Louisville, Louisville, KY 40292

Reviewed, accepted September 23, 2010

Abstract

Joints between dissimilar material systems made using laser metal deposition processes have been investigated. The fusion of materials with different physical properties and chemical compositions under high laser power often results in defects at the joints. Although some solutions have been suggested in previous work for defect-free fabrications, most of the joints studied have been characterized using qualitative techniques only. Quantitative study is imperative for predicting the mechanical behavior of fabricated structures for real life applications. In this work, tensile and flexural specimens made of different Ti6Al4V and Ti6Al4V/10%TiC dual-material transition joint designs were fabricated using laser engineered net shaping (LENS) and tested. It was found that transition joint design has a significant effect on the tensile strengths of dual-material structures.

1. Introduction

The capabilities of additive manufacturing (AM) technologies to fabricate complex geometries have been widely demonstrated. AM has also been shown to enable the fabrication of heterogeneous materials and microstructural mixes in a single component. Some technologies like 3D printing [1-2], stereolithography [3-4], selective laser sintering [5], ultrasonic consolidation [6-8], direct laser metal deposition processes [8-11] and others have been used to demonstrate the multi-material capabilities of AM. The materials used range from polymers to metals and ceramics; and in some cases are process-specific. The chemical and physical compatibilities of the material systems are important factors that determine the qualities of the joint between multiple materials. The use of difficult-to-join material systems is a challenge, however several solutions have been shown to enable the successful. Two examples are the use of gradient transitions from one material to the other [12] and the use of compatible intermediate materials [7].

Inter-material joint problems are common in fusion-based processes such as direct laser metal deposition processes. The processes include laser engineered net shaping (LENS) and its variants, like direct light fabrication (DLF), epitaxial laser metal forming (E-LMF), laser direct forming (LDF), laser rapid forming (LRF) and others. Good selection of process parameters are required in order to achieve defect free component fabrication in all cases.

LENS possesses the capabilities to fabricate fully dense structures using powder materials. It fabricates solid objects in a layer-wise fashion from computer aided design (CAD) models that are first numerically sliced to predetermined thickness. Each layer is fabricated by melting powder materials delivered to the focus of the laser beam on a substrate that is mounted on an x-y stage. The stage moves in a raster fashion according to the tool paths generated using

the sliced CAD models. The fabrication takes place under a controlled, inert atmosphere in a glove box. The process is schematically illustrated in Fig. 1. Some of the important process parameters are laser power, powder flow rate, layer thickness, hatch width, deposition speed and oxygen level in the glove box. The capabilities of the process for multi-material fabrication have been demonstrated. It is used for composite material fabrication [13-14], functionally gradient structures [11-12], multi-materials processing [10] surface cladding for corrosion resistance [11], and biomedical applications [15-16].

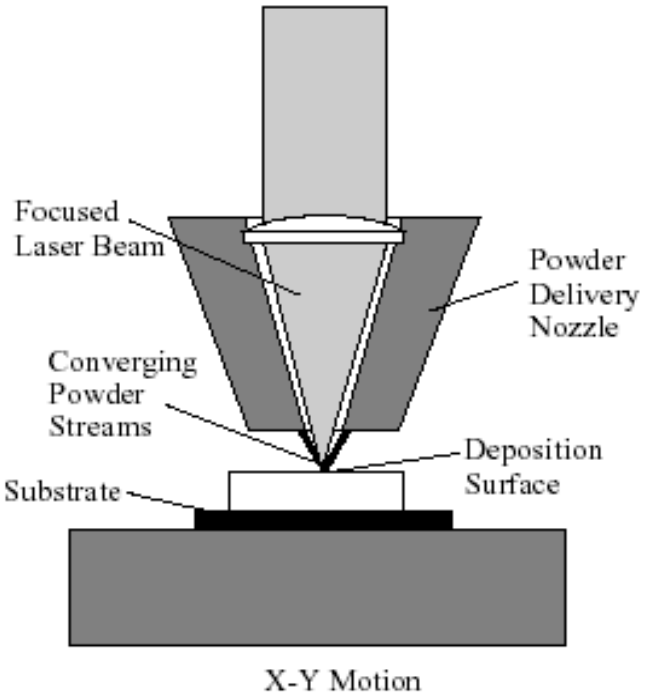

Figure 1: Schematic illustration of LENS deposition process

Most of the earlier work on multi-material fabrication using direct laser metal deposition processes does not go beyond establishing successful fabrication of different material systems through qualitative characterizations using microstructure studies. However, its potential for

fabricating multi-material structures for load carrying applications will not be fully achieved without establishing the mechanical properties of transition joints between the materials.

Dual-material minimum weight structure design [17-19] is one of the evolving application areas of AM fabricated multi-material structures. They are both geometrically and materially complex, and thus are difficult or impossible to fabricate using conventional processes. They are made of multiple, thin members that are preferably made from light weight materials with high specific strength and stiffness. Such structures are readily applicable to aerospace and automotive industries, where there is continuous emphasis on higher strength and lower weight structures for improved fuel efficiency and performance. Figure 2 shows an example of a complex minimum weight structure with members that could be made of different materials based upon Michell theory [21]. In the illustrated structure, if the structure is pinned at points A and B and a load is placed at C, parallel to a line between A&B, as shown with the arrow, the outer member labeled D will be in pure compression, as well as all the inner members that join D tangentially. Those inner network members that are perpendicular to D, and the member between A and C will be in pure tension. In order to optimize a structure to its fullest extent, the members in tension can be made of materials different from those in compression. In this case, the intersection between the tensile and compressive members and the design and strength of these joints is of critical importance for the structure's reliability and performance.

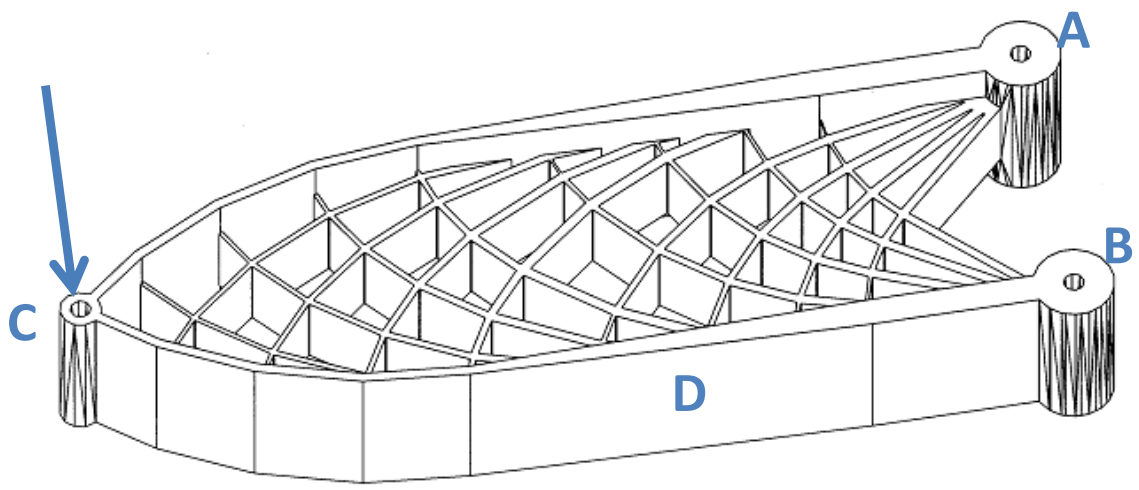

Figure 2: A minimum weight structure design [21]

Simplified minimum weight structures that are representative of the more complex design shown in Fig. 2 were designed based on maximum strength and maximum stiffness criteria [17] and fabricated. Figure 3 shows a free body diagram of a simplified structure design with *oa*, *ob* and *oc* as compression members and *ab* and *ac* as tension members when subjected to compressive load *F* with simple supports at *b* and *c*. Given such a design with

span = L,

applied force = F,

$$F = f\sqrt{2}\ ,$$

where, f is the stress acting on the tension members at any point during loading, Table 1 shows the load relationships existing in the structure members. Structures designed based on maximum stiffness criterion must satisfy the following strain ratio [17].

$$\frac{\varepsilon_T}{\varepsilon_C} = \left[\frac{\left(\rho_T / E_T\right)}{\left(\rho_C / E_C\right)}\right]^{\frac{1}{2}} = \left(\frac{E_C \rho_T}{E_T \rho_C}\right)^{\frac{1}{2}} \qquad \text{(i)}$$

Table 1: Load and size relationship for minimum weight structure

Element	Length	Force	Cross-sectional area
oc	$L/2$	$F/2 = f/\sqrt{2}$	$F/(2\sigma_C)$
oa	$L/2$	$F = f\sqrt{2}$	$F/(\sigma_C)$
ac	$L/\sqrt{2}$	$F/\sqrt{2} = f$	$F/(\sqrt{2}\sigma_T)$

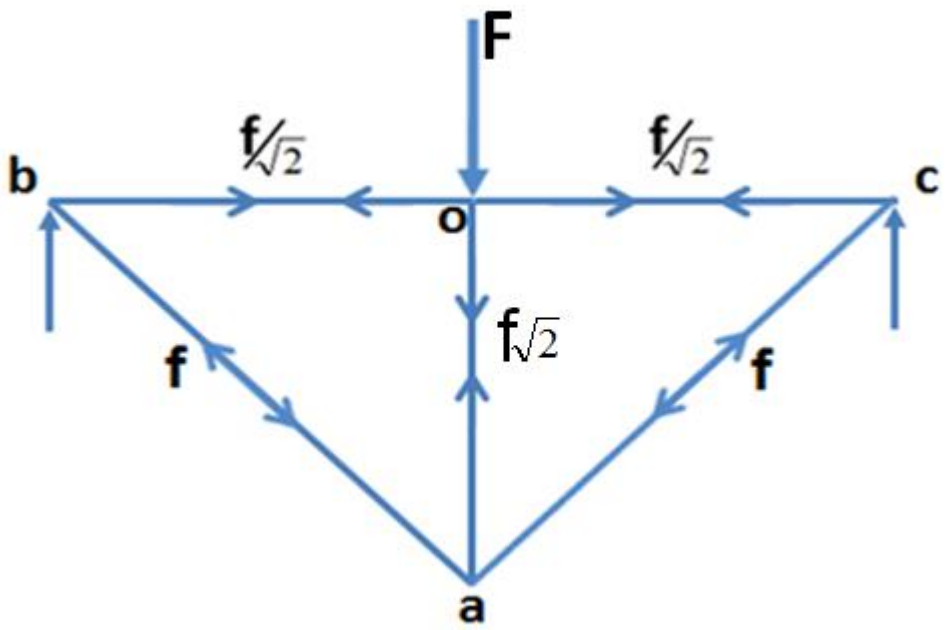

Figure 3: Free body diagram of the dual-material minimum weight structure

This work is aimed at characterizing the failure characteristics and strengths of dual-material systems using different material transition designs at the joints between tensile and compressive members. Ti6Al4V/TiC composite and Ti6Al4V materials were used for the study. Different material transition joints were designed and tested for flexural and tensile strengths. Optimal designs were applied for the fabrication of dual-material minimum weight structures and tested.

2 Experimental Procedures

A laser engineered net shaping (LENS 750) machine made by Optomec Inc., Albuquerque, USA, was used for this experiment. The machine uses a continuous wave ND:YAG laser with a capacity of up to 400 Watts. The laser power used ranged from 200 to 270 Watts. The machine has a dual powder feeder system that allows the simultaneous delivery of two different material mixtures. The powder is delivered by argon carrier gas to the focus of the laser beam, and deposits were made on a 6mm thick commercially pure (CP) titanium substrate. The machine has a 3- axis motion system consisting of an x-y motion stage and a z-axis for integrated laser and powder delivery system. The oxygen level was maintained under 10 parts per million (ppm) in the glove box. Deposition layer were of 0.25mm thickness and 0.38mm hatch width for all fabrications.

Spherical Ti6Al4V powder material of 125 – 210 microns diameter supplied by Advanced Specialty Metals (ASM), New Hampshire, USA and TiC powder of 45 – 150 micron particle size, supplied by Pacific Particulate Materials (PPM) Limited, Canada, were. Although the recommended powder particle size for LENS fabrication is 45 – 150 microns diameter, the Ti6Al4V size used was found to flow well through the delivery system. Two sets of dual-

material specimens were fabricated for joint strength characterization. A set was fabricated for flexural strength determination and another set of corresponding joint designs for tensile properties determination.

In each test type, six different joint designs were fabricated with three replicates. The designs, as shown in Fig. 4 below are: butt joint; gradient transition joint; interlocked material joint, randomly interlocked material joint, scarf joint and v-groove joint. The joints are respectively labeled butt, gradient, interlock, random, scarf, and v-groove in this work. The specimens were fabricated with Ti6Al4V material at one end and Ti6Al4V/10wt%TiC at the other. The joint designs define the transition from one material to the other. The butt joint was designed for an abrupt transition from one material to the other. Interlock joints were fabricated with interlocking strips of materials of 1mm thickness. They were made by depositing four layers of materials for each strip. Random joints were designed with random lengths of interlocking strips of 0.5mm. They were made by depositing two layers of materials for each strip. The scarf joint was designed with a lap angle of 45^{o} while the included angle of the v-groove joint design is 90^{o}. The v-groove specimens were fabricated by first depositing the two principal materials completely, and the groove subsequently filled up with the transition material. In this work, the groove filler material was Ti6Al4V, one of the two principal materials. The gradient transition joint was designed to vary TiC composition linearly from zero to 10wt%TiC in Ti6Al4V at a step interval of 0.25mm over a total length of 5mm.

Material-specific STL CAD files were developed for the fabrication of the dual-material test specimens. Two different material mixtures were automatically deposited side-by-side for each layer following the spatial relationship specified in the machine code, which was dependent on the joint design. The gradient transition joint specimens were fabricated with orientations

parallel to the deposition z-axis direction, as more than three axes would be required for its deposition in any other direction. Specimens with other joint designs were deposited with orientations perpendicular to the deposition nozzles. Single material specimens were fabricated to determine the as-deposited tensile properties of the two base material mixtures (Ti6Al4V and Ti6Al4V/10wt%TiC). A combination of computer numerical control (CNC) milling and wire electrical discharge machining (EDM) were used to finish up the specimens to final size and to remove them from the substrate.

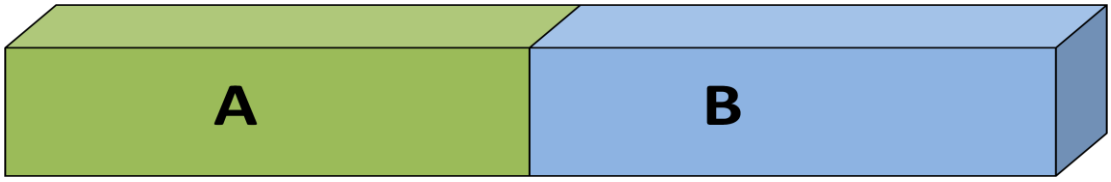

(a) Butt joint

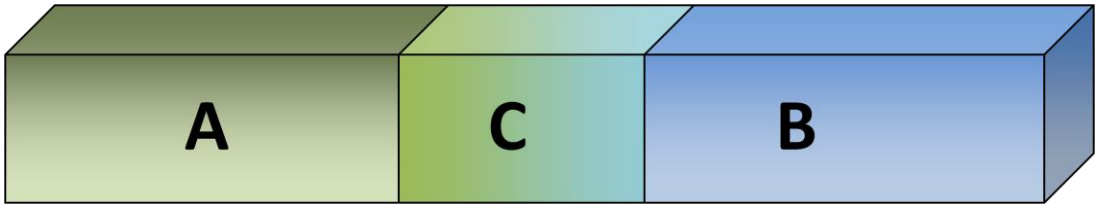

(b) Gradient joint

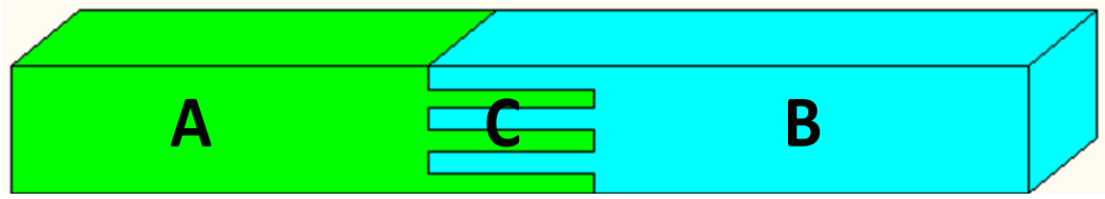

(c) Interlocking joint

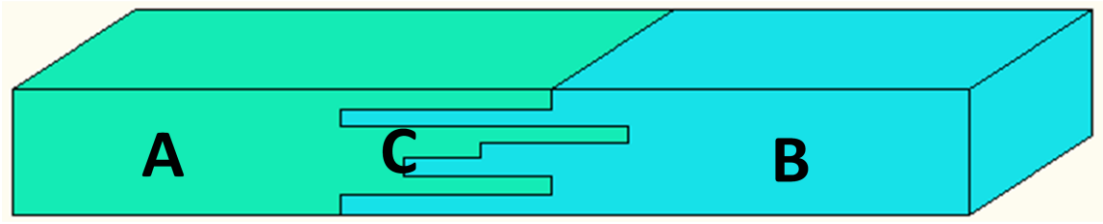

(d) Random interlock joint

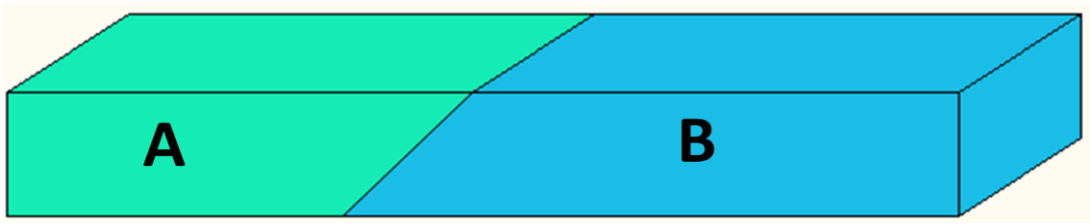

(e) Scarf joint

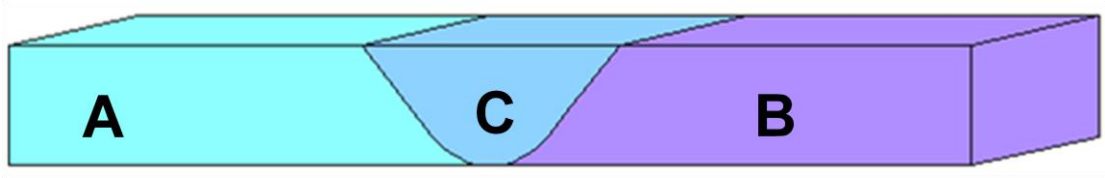

(f) V-roove joint

Figure 4: Multi-material interface designs for LENS deposition

All tensile specimens were made in accordance with ASTM E 8_E 8M. 3-point bend specimens were sized based on ASTM C1341-06. The flexural strengths were calculated using

$$\sigma_f = \frac{3FL}{2bd^2} \qquad \text{(ii)}$$

where, σ_f = flexural strength

F = load at failure

L = specimen support span

b = specimen width, and

d = specimen thickness.

An ASTM D 2344 short beam 3-point test fixture was used for the flexural strength tests. A 50kN Tinius Olsen tensile testing machine was used for all tests at a crosshead speed of 0.5mm/minute.

Dual-material minimum weight structures designed based upon maximum strength and maximum stiffness criteria were fabricated using selected material transition joint designs. This selection was based on the results of the joint design characterizations just described. The structures were meant to test the performance of the joint designs in practical applications. They were fabricated using Ti6Al4V as the compression member material and Ti6Al4V/10wt%TiC as the tension member material. Depending on the application, the compression and tension member materials as specified can be maintained or reversed. The Ti6Al4V/10wt%TiC was selected for the tension members in anticipation of higher tensile strength than Ti6Al4V. Members subjected to tension fails faster than compression members under loading conditions. The use of the composite material in the tension members was intended to increase load carrying capability before failure of the structure. An initial attempt to fabricate the structures with Ti6Al4V/10wt%TiC composite as the tension member using the T- and V-shaped material models shown in Fig. 5 was unsuccessful as cracks developed during deposition, mostly after the eighth layer. The cracks initiated and propagated at the Ti6Al4V/10wt%TiC composite side at the joints. Butt and scarf joints shown in Fig. 5 were used during those trials. The labels A and B indicate mating surfaces of the T- and V- geometries during deposition to form the final shape. The cracks developed irrespective of the joint design used. However, structures fabricated with 5wt%TiC composition in the tension material member did not crack.

The problem with cracks necessitated a change in the design of the material models to allow for a combination of butt and interlock joints at all the material intersections as shown in Fig. 6. Figure 6a is a fork shaped Ti6Al4V material model with arms extending through the triangular shaped structure. The two lower arms in Fig. 6 are of 0.5mm thickness, while the topmost arm is of 1mm thickness. The arms were intended to separate Ti6Al4V/10wt%TiC composite tension members (with material model shown in Fig. 6b) into three discrete partitions with Ti6Al4V as 0.5mm thick inter-layers. However, during the fabrication, rather than deposit two layers of Ti6Al4V materials consecutively at the inter-layer, they were alternated with Ti6Al4V/10wt%TiC composite layers. This deposition method significantly reduces the occurrence of cracks in the deposits. Fabricated minimum weight structures were tested with an ASTM D 2344 short beam test fixture as illustrated in Fig. 7. The load at failure was obtained for analysis. Also, the mode of failure, especially the fracture location, was studied.

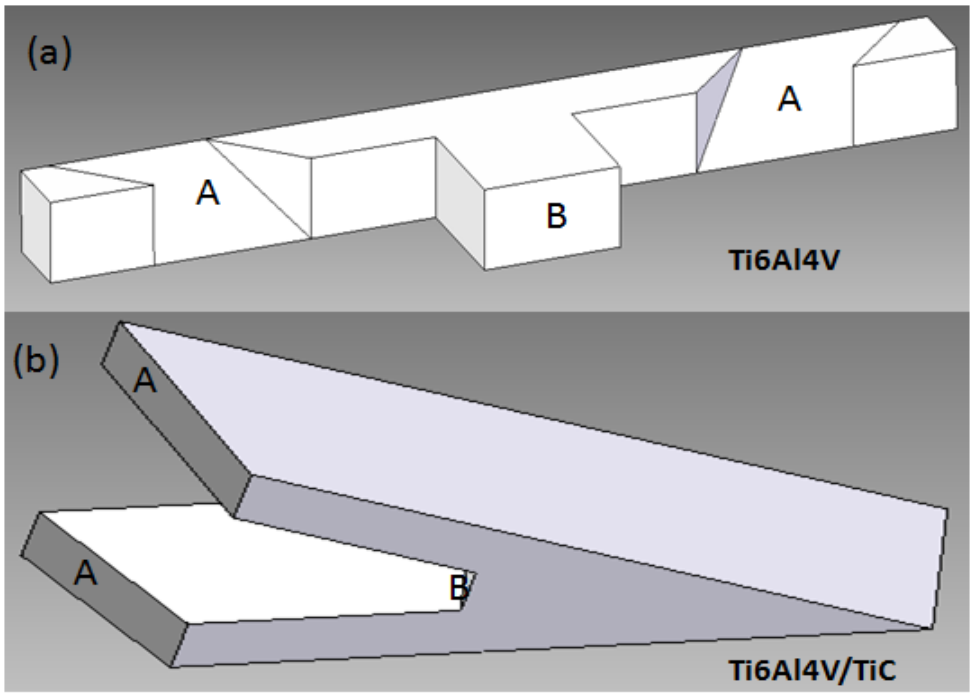

Figure 5: T- and V-shaped CAD material models

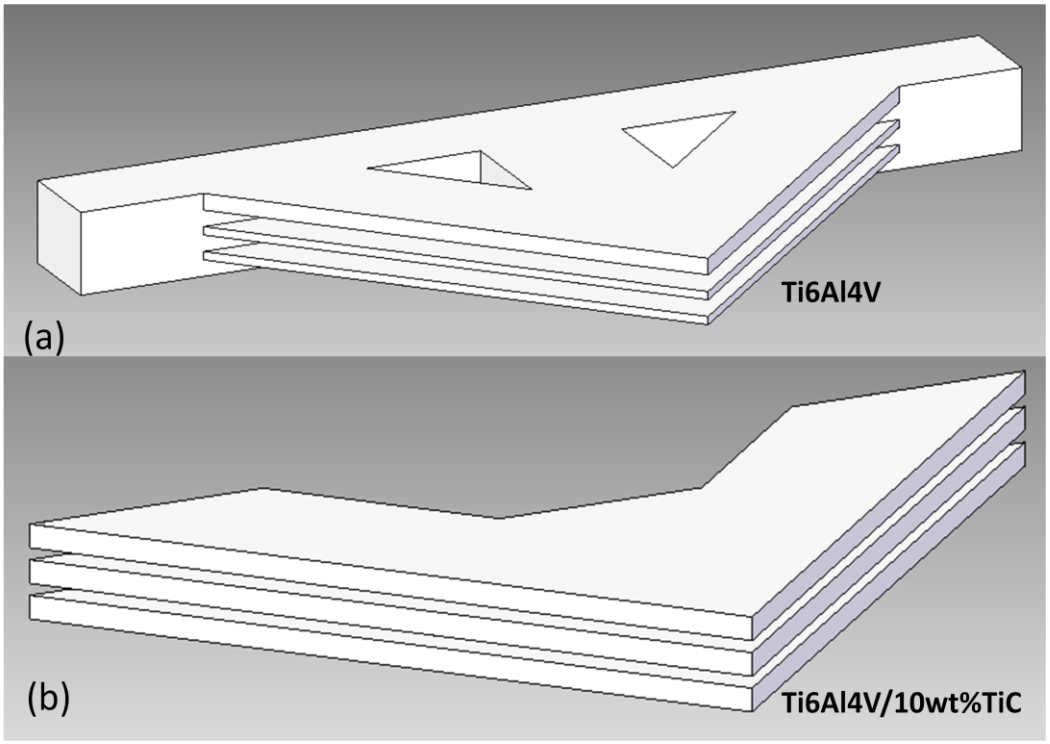

Figure 6: Material specific CAD models

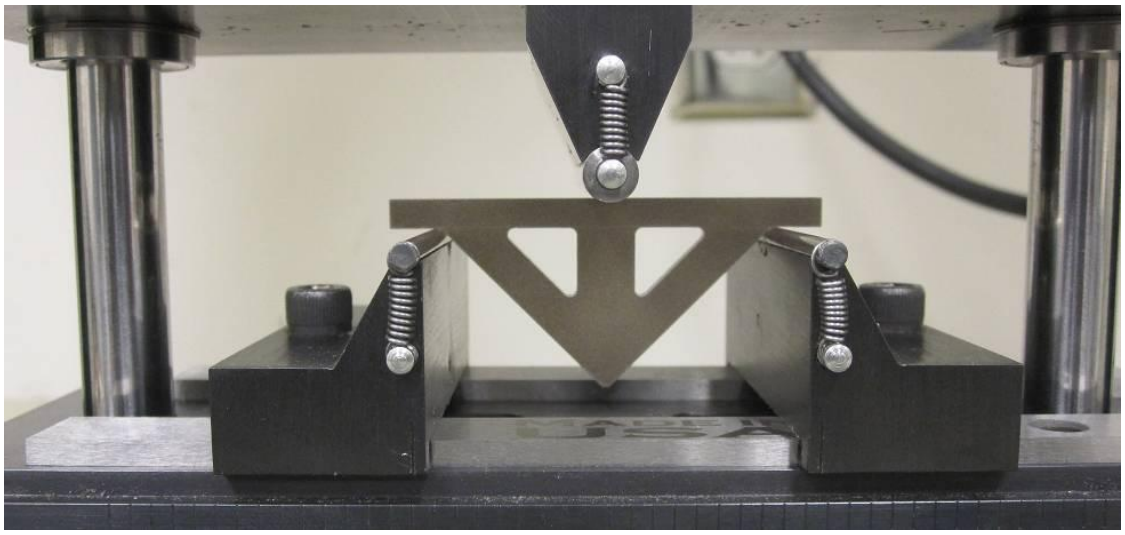

Figure 7: Structure under test using a 3-point bend test fixture

6.3 Results and Discussion

3.1 Microstructures

Some of the micrographs of deposited specimens are shown in Fig. 8 below. Figure 8a shows a micrograph of Ti6Al4V/10wt%TiC deposit. Figure 8b and 8c shows the butt joint interface with some level of interlock. The interlock is due to the fact that the two material models used for the dual material specimens share the same contour boundary line, and in every layer, each of the materials is deposited at the common boundary resulting in small amount of interlock. A gradual transition from one material to the other can be observed in Fig. 8c. Figures 8d and 6.8e shows sandwiched strips of Ti6Al4V/10wt%TiC composite and Ti6Al4V materials in an interclock material joint. The micrograph of a scarf joint is shown in Fig. 8f.

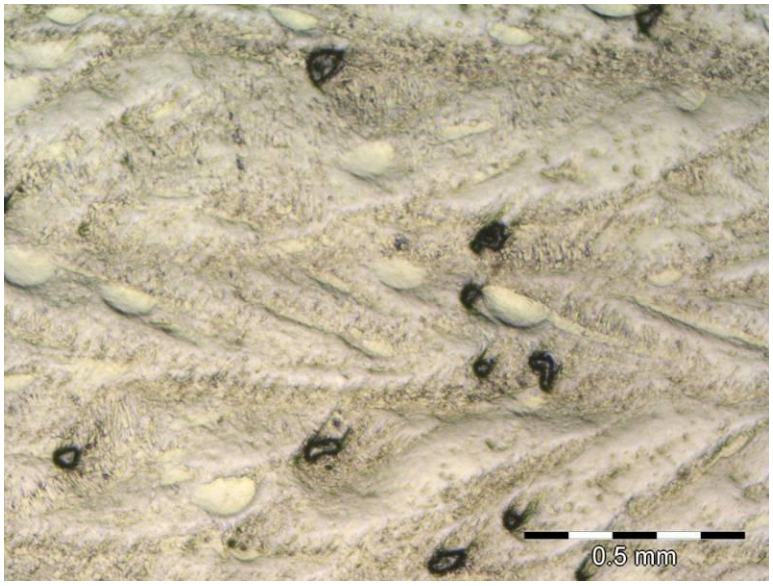

(a): Ti6Al4V/10wt%TiC composite showing some un-melted particles

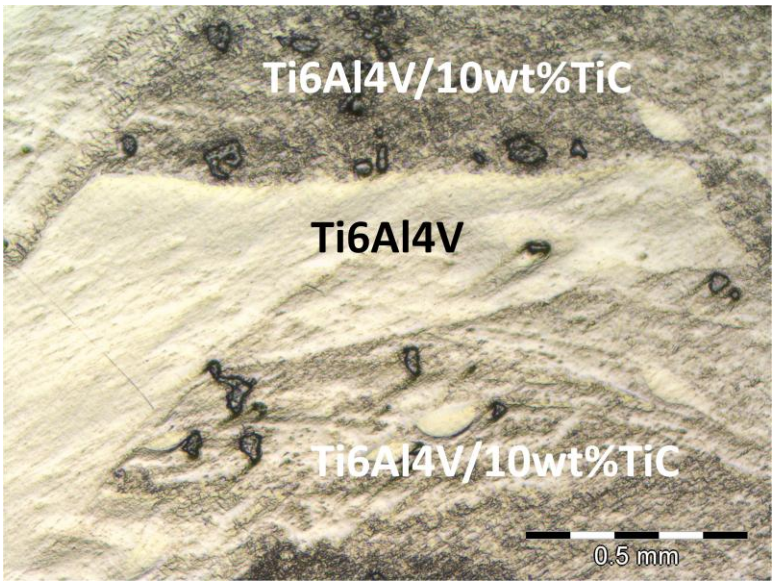

(b): Butt joint showing small interlock at the boundary contour deposit

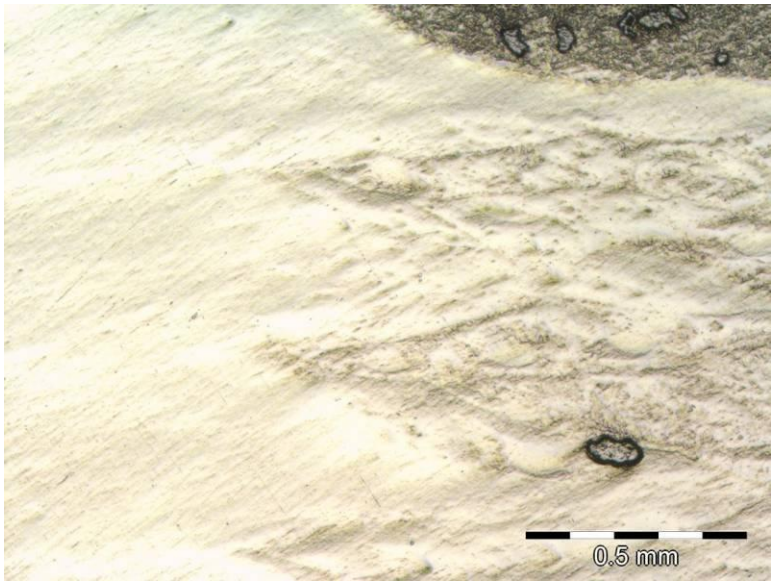

(c): Butt joint showing material mixing at the interface

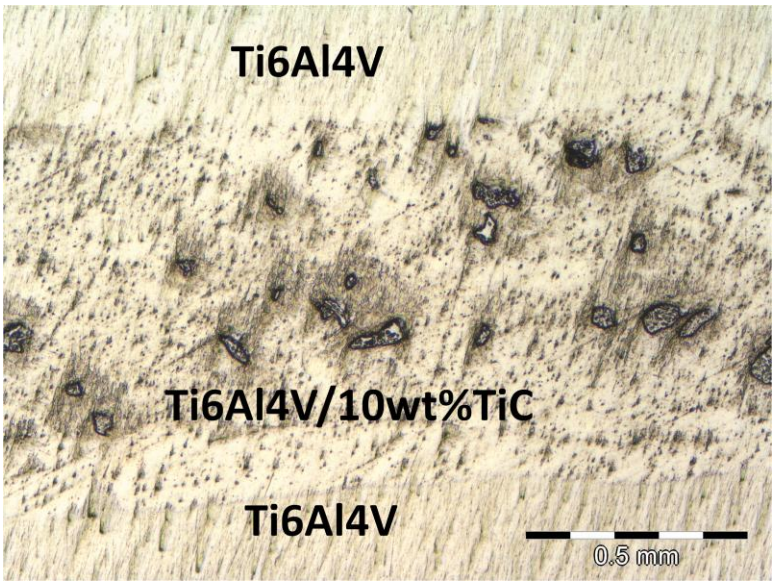

(d): Interlocked joint showing a sandwiched Ti6Al4V/10wt%TiC strip

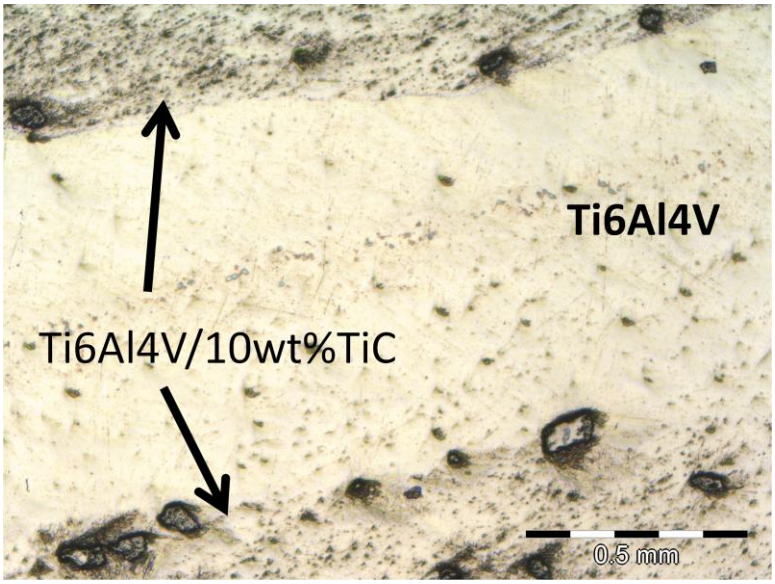

(e): Interlocked joint showing a sandwiched Ti6Al4V strip

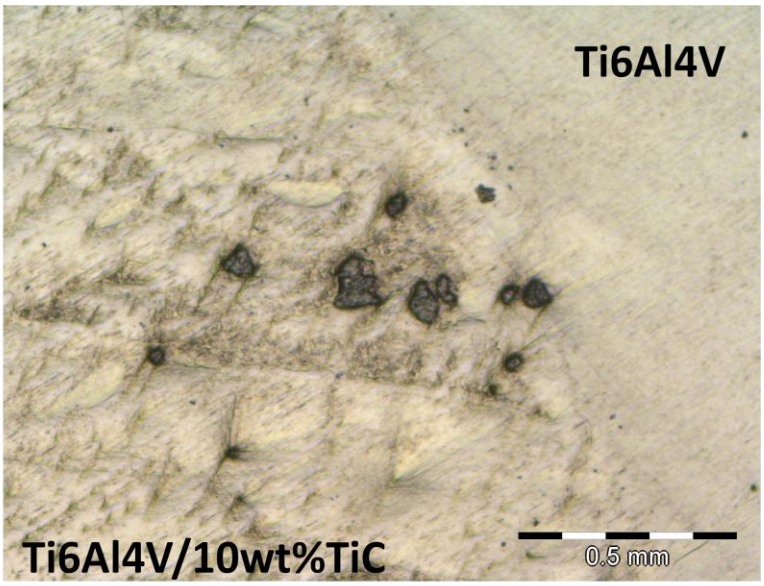

(f): Scarf joint showing the interface between Ti6Al4V/10wt%TiC and Ti6Al4V

Figure 8: Micrographs of some of the dual-material test specimens

3.2 Flexural and Tensile Strengths

The flexural strength data obtained are shown in Table 2 and graphically in Fig. 9. The flexural strengths of the base materials (Ti6Al4V and Ti6Al4V/10wt%TiC) are included. It can be seen from the data that under the bending load condition, the scarf joint design yielded the highest average flexural strength. It also has one of the lowest strength variations. The butt joint design yielded the lowest average strength. The result of a statistical analysis of the data using SAS 9.1 show that joint design (with a p-value of 0.2268) does not have statistically significant effect on the flexural strength of the LENS fabricated specimens. It means for an application requiring lateral loading, any of the inter-material joint designs can be used. The ease of fabrication will therefore be a major consideration for such applications.

The tensile strengths data for corresponding joints designs are shown in Table 3 and Fig. 10. The results of the analysis of the data show that joint design has a statistically significant

effect on the tensile strengths of LENS fabricated dual-material structures with a low p-value of 0.0002 as shown in the analysis of variance (ANOVA) Table 4a. Single material specimens with Ti6Al4V and Ti6Al4V/10wt%TiC expectedly have the highest average tensile strength values. According to the Ryan-Einot-Gabriel-Welsch (REGWQ) post hoc means analysis table shown in Table 4b, both interlock and butt joint designs have statistically significantly higher average tensile strengths than random and v-groove designs. Although the former pair yielded higher average tensile strengths than gradient and scarf joints, the differences are not statistically significant. It means any of those four designs can be used in place of another in LENS fabricated dual-material structures. One of the major defects that might have resulted in low tensile strengths recorded for the v-groove joint design is shown in Fig. 11. In this design, the two principal materials are first deposited completely before the transition joint material is deposited in the groove. With the as-deposited rough surfaces of the principal materials, sometimes the laser does not have all the surfaces exposed for re-melting and deposition with the transition material. Voids are therefore created in the process. The voids act as stress raisers that cause weakening of the joints and early failure.

Table 2: Flexural Strength (MPa) Data

Material/Joint Design	Samples 1	2	3	Average
Butt	1790.04	1686.56	1264.48	1580.36
Gradient	1996.37	1875.49	2003.27	1958.38
Interlock	1864.19	2389.45	1837.56	2030.40
Random	1885.64	1610.98	1865.32	1787.31
Scarf	2093.81	2091.60	2251.95	2145.79
Ti64	2163.86	1895.14	1896.96	1985.32
Ti64/10wt%TiC	1578.96	2033.35	1388.11	1666.81
V-Groove	1449.64	2026.20	2422.69	1966.18

Table 3: Tensile Strength (MPa) Data

Material/Joint Design	Samples 1	2	3	Average
Butt	1138	1124	1096	1119.33
Gradient	1055	1080	1035	1056.67
Interlock	1186	1163	1090	1146.33
Random	855	935	834	874.66
Scarf	1089	1021	1034	1048.00
Ti64	1119	1196	1192	1169.00
Ti64/10wt%TiC	1225	1240	1124	1196.33
V-Groove	770	978	1069	939.00

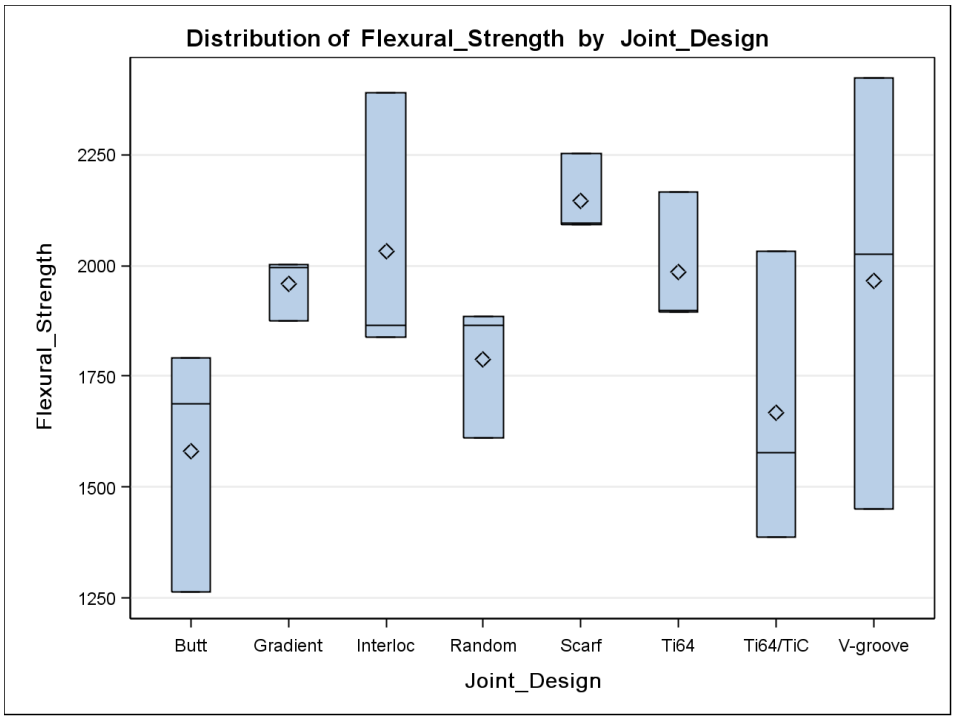

Figure 9: Comparison of flexural strengths (MPa) of LENS fabricated dual-material joint designs

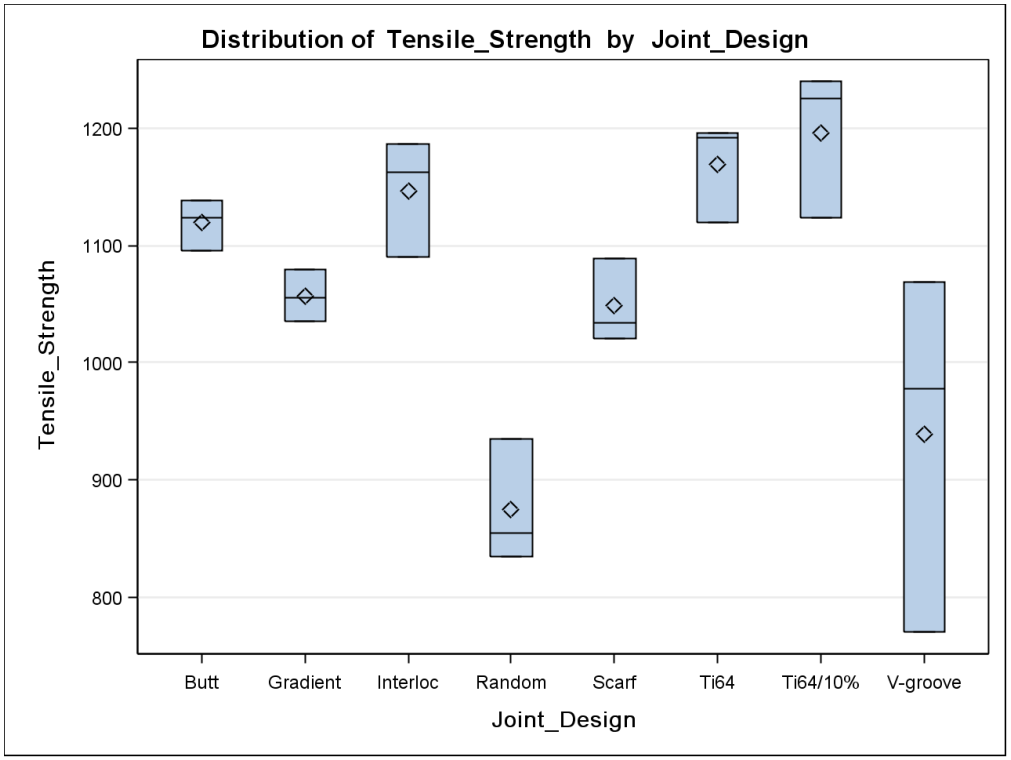

Figure 10: Comparison of tensile strengths of LENS fabricated dual-material joint designs

Table 4a: Analysis of Variance

Source	DF	Type III SS	Mean Square	F Value	Pr > F
Joint_Design	7	269956.0000	38565.1429	8.34	0.0002

Table 4b: REGWQ Multiple Range Test for Tensile Test Data

Means with the same letter are not significantly different.				
REGWQ Grouping		Mean	N	Joint_Design
	A	1196.33	3	Ti64/TiC
	A			
	A	1169.00	3	Ti64
	A			
	A	1146.33	3	Interlock
	A			
	A	1119.33	3	Butt
	A			
B	A	1056.67	3	Gradient
B	A			
B	A	1048.00	3	Scarf
B				
B	C	939.00	3	V-groove
	C			
	C	874.67	3	Random

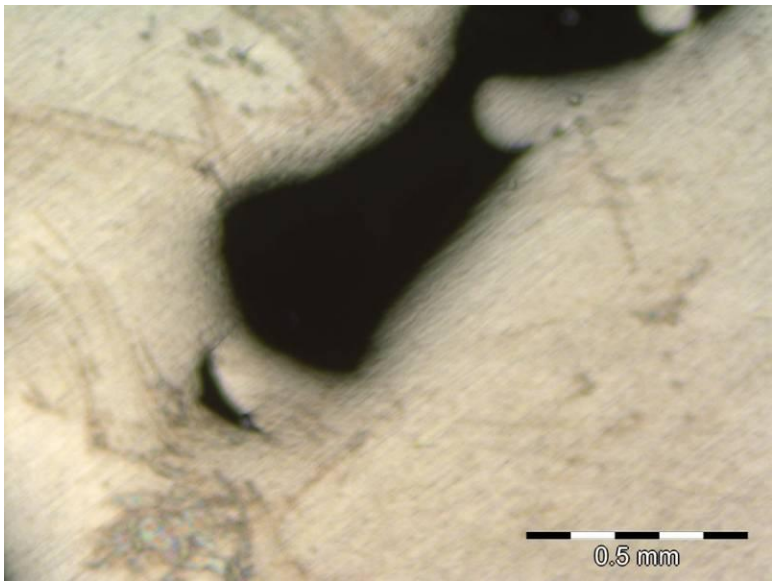

Figure 11: Defect on a V-groove joint design

3.3 Dual-Material Minimum Weight Structures Test Results

A sample of the fabricated minimum weight structures is shown in Fig. 12. The joint locations are marked with letters A and B. Data obtained from the loading tests are shown in Tables 6 to 8. For ease of representation, the structures are labeled as follows: the maximum strength criterion structures with 5wt%TiC in the tension members are denoted STR5; the maximum stiffness criterion structures of the same composition are STF5; and the corresponding structures with 10wt%TiC are STR10 and STF10. Table 5 shows the member (*oa*, *oc* and *ac* illustrated in Fig. 3) sizes for each of the fabricated structures.

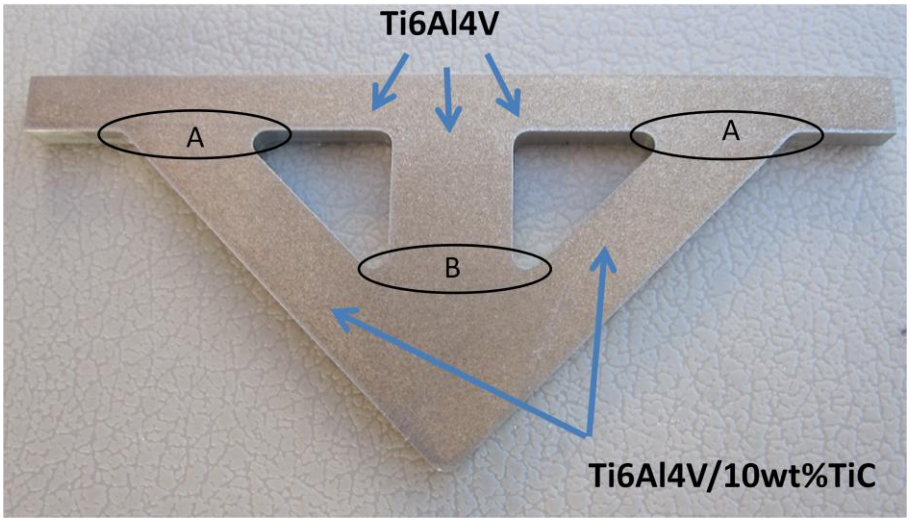

Figure 12: LENS fabricated dual-material minimum weight structure

Table 5: Member sizes for fabricated minimum weight structures

Structure	Sample	Member width (mm)			Thickness
		oa	***oc***	***ac***	
STR5	1	8.00	4.00	6.00	3.20
	2	8.00	4.00	6.00	3.20
	3	8.00	4.00	6.00	3.20
STF5	1	7.14	3.57	6.40	4.00
	2	7.14	3.57	6.40	3.60
	3	7.14	3.57	6.40	4.00
STR10	1	8.00	4.00	5.50	2.90
	2	8.00	4.00	5.50	3.00
	3	8.00	4.00	5.50	2.84
STF10	1	7.00	3.50	4.77	3.25
	2	7.00	3.50	4.77	3.35
	3	7.00	3.50	4.77	3.39

Table 6: Failure loads (kN)

Structure	Samples			Average
	1	2	3	
STR5	13.87	7.44	12.77	11.36
STF5	21.3	13.06	18.14	17.50
STR10	14.2	11.81	13.25	13.08
STF10	12.1	13.76	14.96	13.61

Table 7: Stresses (MPa) acting on the tension members at the time of failure

Structure	Samples			Average
	1	2	3	
STR5	511	274	470	418.33
STF5	588	401	501	496.67
STR10	630	506	600	578.67
STF10	552	609	654	605.00

Table 8: Strain energy densities (J/m^3) data for LENS fabricated minimum weight structures

Structure	Samples			Average
	1	2	3	
STR5	1.24E+6	3.56E+5	1.05E+6	881,452.8
STF5	2.00E+6	9.28E+8	1.45E+6	1,458,924
STR10	1.51E+6	0.975E+6	1.37E+6	1,284,867
STF10	1.15E+6	1.40 E+6	1.61E+6	1,385,939

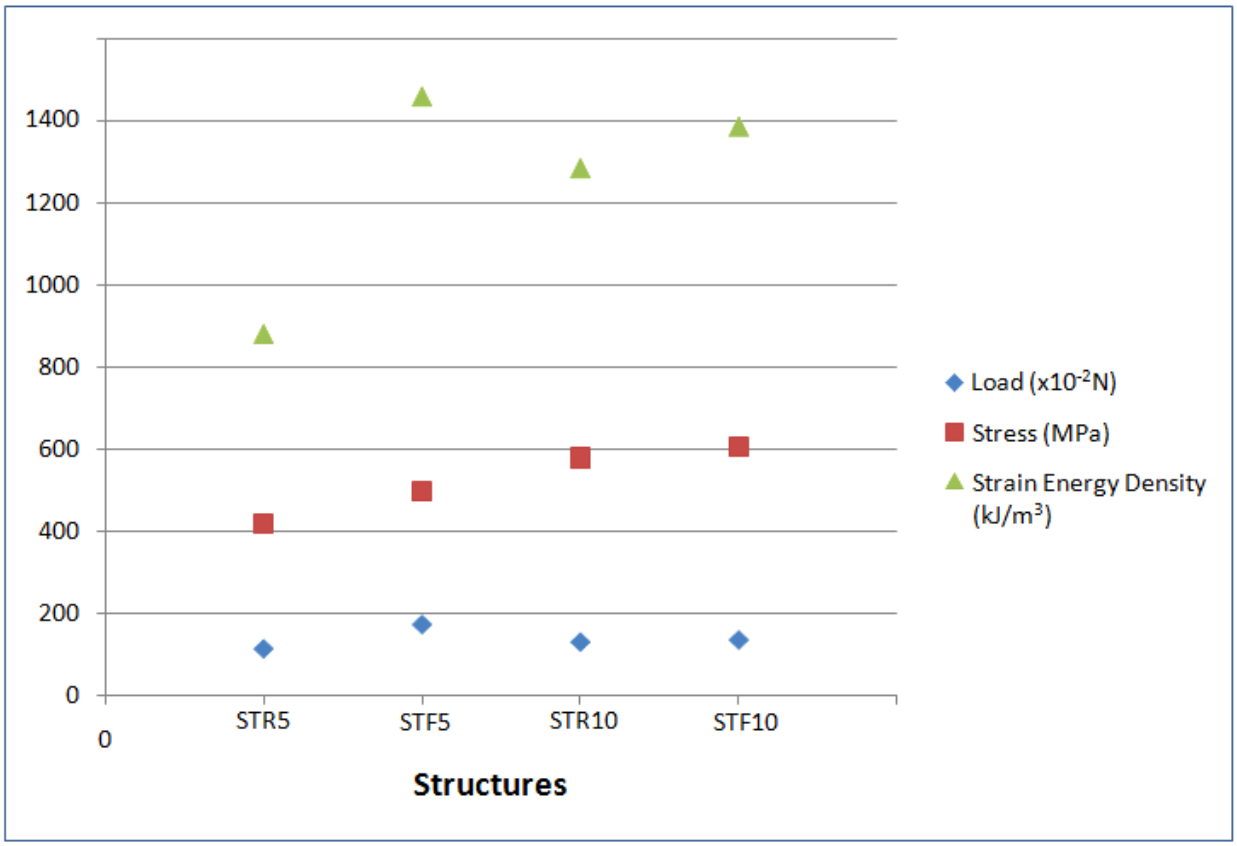

Figure 13: Loads, stresses and strain energy densities at failure in the structures

The load *F* (as illustrated in Fig. 3) applied at the time of failure for each structure is shown in Table 6. Table 7 shows the stress on the tension members at failure, while Table 8 shows the calculated strain energy density for each structure. The load applied at failure for both material composition structures, seen graphically in Fig. 13, are close in value, although they are not directly comparable since they are of different thicknesses. The stresses on the tension members (*ac* or *ab* in Fig. 3) for each structure are shown in Table 7 and Fig. 13. STR10 and STF10 structures failed at slightly higher stresses in the tension members than corresponding STR5 and STF5 structures. The stress values are about 50% of the tensile strength of the respective materials. The tensile strengths as experimentally determined are shown in Table 9. It

is noteworthy that no failure occurred at the joints in any of the structures irrespective of the TiC composition used.

Table 9: Average Tensile properties of materials used

Material	Yield strength (MPa)	Tensile strength (MPa)	Modulus (GPa)
Ti6Al4V	1072	1169	111
Ti6Al4V/5wt%TiC	985	1099	114
Ti6Al4V/10wt%TiC	1089	1196	154

Strain energy densities shown in Table 8 were calculated based on the structure member sizes, material properties and strain values using

$$U = \frac{\sum(\frac{1}{2}\sigma\varepsilon v)}{V} \qquad \text{(iii)}$$

Where, U = strain energy density of a structure at failure load

σ = stress in each member at the failure load

ε = strain of each member at failure load

v = volume of each structure member

V = total volume of the structure being analyzed

The stress σ in each member at the point of failure was calculated by normalizing the resolved load (based on Table 1 relationships) with respect to cross-sectional area. With the stress obtained, the strain ε was calculated using the stiffness value for each structure member.

The strain energy density data shows that the structures designed based on maximum stiffness criterion generally yielded higher average strain energy density than those designed

based on maximum strength criterion for both tension member material compositions (5wt% TiC and 10wt%TiC). This result is opposed to the results obtained in earlier work [20] in which ultrasonically consolidated structures based on maximum strength criterion yielded significantly higher average strain energy density than those designed based on maximum stiffness criterion. Most of the structures in the referenced work failed at the foil edge-to-edge joints at the tension members as opposed to failures at the flanges for most of the LENS fabricated structures. It was for only one case that the maximum strength criterion structure failure occurred at one of the tension members, as shown in Fig. 14a. In all other cases, both for maximum strength and maximum stiffness criteria, failures occurred at the flanges as shown in Fig. 14b.

(a): Failure at a tension member on an STR10 structure

(b): Failure at the flange obtained in most structures

Figure 14: Fracture locations in LENS fabricated minimum weight structures+

4 Conclusions

It has been shown experimentally in this work that transition joint design does not have significant effect on the flexural strengths of LENS fabricated dual-material structures made of compatible materials. In contrast, joint design has significant effect on their tensile strengths. V-grooved and randomly interlocked joint designs yield poor tensile strengths when compared to interlocked, butt, gradient and scarf joints. Among the later four design types, the interlock design yielded the best average tensile strength. It also performed well under flexural loading. However, any of the four designs can be used for structural applications. None of the LENS fabricated minimum weight structures fail at the material transition joints under 3-point loading conditions. This work has shown that several different types of joint designs may work reliably for multi-material components.

References

1 Cohen D.L., Malone E., Lipson H. Bonassar L.J., 2006, "Direct Freeform Fabrication of Seeded Hydrogels in Arbitrary Geometries", Tissue Engineering, **12**(5), pp.1325-1335.

2 Malone E., Rasa K., Cohen D., Isaacson T., Lashley H., Lipson H., 2004, "Freeform Fabrication of Zinc-air Batteries and Electromechanical Assemblies", Rapid prototyping journal, **10**(1), pp.58-69.

3 Inamdar A., Magana M., Medina F., Grageda., Wicker R. "Development of Automated Multiple Material Stereolithography Machine", Proceedings of Solid Freeform Fabrication Symposium, Austin, TX, USA, August 2006.

4 Jae-Won Choi J., MacDonald E., and Wicker R. "Multiple Material Microstereolithography", Procedings of Solid Freeform Fabrication Symposium, Austin, TX, USA, August 3-5, 2009

5 Liew C.L., Leong K.F., Chua C.K. and Du Z., 2001, "Dual-Material Rapid Prototyping Techniques for the Development of Biomedical Devices. Part 1: Space creation", The international Journal of Advanced Manufacturing Technology, **18**(10), pp.717-723

6 Janaki Ram G.D., Robinson C., Yang and Stucker B.E., 2007, "Use of Ultrasonic Consolidation for Multi-Material Structures", Rapid Prototyping Journal, **13**(4), pp.226-235.

7 Obielodan J.O. , Ceylan A., Murr L.E. and Stucker B.E., 2010, "Multi-Material Bonding in Ultrasonic Consolidation", Rapid Prototyping Journal, **16**(3), pp. 180-189.

8 Obielodan J.O. and Stucker B.E., "Effects of Post Processing Heat Treatments on the Bond Quality and Mechanical Strength of Ti/al3003 Dual-Materials Fabricated using Ultrasonic Consolidation" , Proceedings of Solid Freeform fabrication Symposium, Austin, TX, USA, August 3-5, 2009.

8 Choi J. and Chang Y., 2005, "Characteristics of laser aided direct metal/material deposition process for tool steel", International Journal of Machine Tool and Manufacture, **45**, pp.597-607.

9 Wang F., Mei J., Jiang H., Wu X, 2007. "Laser Fabrication of Ti6Al4V/TiC Composites using Simultaneous Powder and Wire Feed", Materials Science and Engineering A, **445-446**, pp.461-466

10 Griffith M.L., Harwell L.D., Romero J.T., Schlienger E., Atwood C.L., Smugeresky J.E., "Multi-Material processing by LENS", Proceedings of the Solid Freeform Fabrication Symposium, August 1997, Austin, TX, PP.387

11 Lin X, Yue T.M., Yang H.O. and Huang W.D., 2006**, "**Microstructure and Phase Evolution in Laser Rapid Forming of a Functionally Graded Ti–Rene88DT alloy", Acta Materialia, **54**(7), pp.1901-1915.

12 Foroozmehr E., Sarrafi R., Hamid S. and Kovacevic R., "Synthesizing of Functionally Graded Surface Composites by Laser Powder Deposition Process for Slurry Erosion Applications", Solid Freeform Fabrication Symposium, Austin, TX, USA, August 3-5, 2009.

13 Banerjee R., Collins P.C., Genc¸ A., and Fraser H.L., 2003, "Direct Laser Deposition of in situ Ti_ 6Al_ 4V_ TiB composites", Materials Science and Engineering A, **358**, pp.343-349

14 Banerjee R., Collins P.C. and Fraser H.L., 2002, "Laser Deposition of In Situ Ti– TiB Composites", Advance Engineering Materials, **4**(11), pp.847-851.

15 Janaki Ram G.D. Stucker B.E., 2008, "LENS® Deposition of CoCrMo Coatings on Titanium Implant Structures," Journal of Manufacturing Science and Engineering, **130**(2), pp. 024503-1 to 024503- 5, 2008.

16 Janaki Ram G.D., Carson E. Stucker B.E., 2008, "Microstructure and wear properties of LENS® deposited medical grade CoCrMo," Journal of Materials Science: Materials in Medicine, **19**(5), pp. 2105-2111, 2008.

17 Dewhurst Peter, 2005. "A general optimality criterion for strength and stiffness of dual-Material property structures", International Journal of Mechanical Sciences, **47**(20), pp.293-302.

18 Selyugin S.V., 2004. "Some general results for optimal structures", Structural and Multi-Disciplinary Optimization, **26**(5), pp.357-366.

19 Michell, A.G.M., 1904. "Limits of economy of material in frame-structures", Philosophical Magazine, **8**(47), pp.589-597.

20 Obielodan J.O. and Stucker B.E., Multi-material minimum weight structures fabrication using ultrasonic consolidation, Journal of Materials Processing Technology, submitted for review, June 2010.

21 Dewhurst Peter, 2001. Analytical solutions and numerical procedures for minimum-weight Michell structures, Journal of the Mechanics and Physics of Solids, **49**(3) 445 – 467